AIAA JOURNAL
Vol. 46, No. 11, November 2008

Analytical Modeling of Impact Resistance and Damage Tolerance of Laminated Composite Plates

K. Y. Huang*
Crea Mech Company, Ltd., 201203 Shanghai, People's Republic of China
and
A. de Boer† and R. Akkerman‡
University of Twente, 7500 AE Enschede, The Netherlands

DOI: 10.2514/1.34622

The present study is concerned with a fully analytical model for predicting impact resistance and damage tolerance characteristics of laminated fiber reinforced composite plates. The energy balance for damage development during the impact process is established with the help of a localized deformation field, in which various effects such as the anisotropy of the delaminated sublaminates, elastic property degradation due to matrix cracking, multiple delaminations, and membrane deformation within the damage zone are taken into account. This results in upper and lower bounds of the delamination threshold load and a deflection-dependent critical load for stable delamination propagation. On the basis of the conservation of energy principle, simple relationships are found between the resulting damage area and the impact energy as well as the peak impact load. The global buckling load of damaged rectangular plates is derived from the energy-based stability criterion, and the residual ultimate strength is calculated using the von Kármán postbuckling strength theory. The analytical solutions obtained turn out to be capable of providing highly accurate predictions compared with the standard impact and the compression-after-impact experiments of carbon-fiber-reinforced polyetherimide and aromatic polymer composites.

Nomenclature

A = crack area, mm^2, or extensional stiffness matrix, N/mm
B = bending-extension coupling matrix, N
C = compliance of structure, mm/N
c = contact radius, mm
D = bending stiffness matrix, N · mm
D^* = reduced bending stiffness matrix, N · mm
$\bar{D}$ = scalar average flexural rigidity, N · mm
E = elastic modulus, GPa, or energy, J
G_C = critical energy release rate, J/m^2
M = moment per unit length, N
N = midplane force per unit length, N/mm, or number of interfaces
n = number of delaminations
P = load, N
Q = reduced stiffness matrix, GPa
S = damage area, mm^2, or shear strength, MPa
U = bending energy plate, J
u = bending energy infinitesimal element, J/mm^2
w = displacement field, mm
X = longitudinal strength, MPa
Y = transverse strength, MPa
Γ = impact energy transfer factor
ζ = normalized critical buckling load
Λ = dimensionless function for minimization
λ = ellipticity ratio
ξ = bending stiffness reduction, N · mm
σ = stress, MPa
Ω = constant in buckling analysis

Received 16 September 2007; revision received 3 June 2008; accepted for publication 8 July 2008.

*General Manager, Guoshoujing Road 351.
†Professor, Chair of Applied Mechanics, Department of Mechanical Engineering, Post Office Box 217.
‡Professor, Chair of Production Technology, Department of Mechanical Engineering, Post Office Box 217.

I. Introduction

BECAUSE of their exceptional strength and stiffness-to-density ratios and their superior physical properties, composite materials are highly suitable for lightweight structural applications in the aviation and aerospace industries. Initially, composite materials were used only in secondary structures. As knowledge and technology in composite materials have improved, their use in primary structures, such as wings and fuselages, has increased tremendously. However, composite structures are susceptible to foreign object impacts, which can result in barely visible impact damage (BVID) involving matrix cracks and multiple interlaminar delaminations. As BVID is in general difficult to detect with maintenance inspection procedures and can lead to a significant reduction of the compression strength, structural design engineers have to deal with impact resistance and damage tolerance issues to make sure that the structures offer sufficient resistance to impact damage and are able to function safely even with BVID present. Therefore, there clearly exists the need for an accurate prediction method for the impact resistance and damage tolerance characteristics of composite structures to realize the maximum potential benefits of weight saving from composite materials.

The topics of impact resistance and damage tolerance of composite materials have been extensively investigated in the past two decades. However, most studies were restricted to an empirical or numerical approach in which, for example, the finite element method was deployed (see the reviews of Abrate [1], Bartus and Vaidya [2], Cantwell and Morton [3], Elder et al. [4], and Richardson and Wisheart [5]). The analytical approach, which may help elucidate the underlying principles behind various phenomena, received little attention in the literature. One of the analytical solutions was the threshold load for the initiation of delamination growth, proposed by Davies and Robinson [6]. By considering a centrally loaded circular quasi-isotropic plate with a circular midthickness delamination, they found that the energy release rate is independent of the delamination radius and that there exists a delamination threshold load above which the delamination starts to grow without further load increase until another failure mode takes

over. This quasi-static solution of the delamination threshold load was extended to a dynamic solution by Olsson et al. [7], in which inertial effects in the delaminated sublaminates were taken into account. At the same moment, the single delamination was extended to multiple delaminations, which were modeled using isotropic layers of equal thickness. For the rest, the analytical buckling solution for anisotropic rectangular plates was given by Whitney (see Jones [8]). An analytical model, which is in a position to predict the complete process of damage development due to low velocity impact and strength reduction associated with BVID, is not available.

The objective of this study is to develop an analytical model for impact resistance and damage tolerance predictions for laminated composite plates using an energetic approach. The damage development modeling is founded on the energy balance principle that crack extension occurs when the energy available for crack growth is sufficient to overcome the resistance of the material. This leads to the upper and lower bounds of the delamination threshold load as well as a stable delamination propagation load. Subsequently, the resulting damage area is derived in accordance with the principle of conservation of energy. Finally, the global-buckling-related structural performance degradation is modeled using the energy-based stability criterion, which states that the flat form of equilibrium becomes unstable when the work performed by the midplane forces becomes equal to the bending energy of the plate.

II. Improved Delamination Threshold Load

This section presents a new delamination threshold load, which takes into account the anisotropic effects of the delaminated sublaminates and the material degradation due to matrix cracking. The model gives a clear mathematical relationship between the delamination threshold load and the key design variable of composite structures, the laminate layup. The model is based on a single delamination, which leads to the maximum potential energy release as two delaminations can not be initiated exactly at the same time from a statistical viewpoint.

A. Basic Assumptions

To facilitate the analysis, the following simplifications and assumptions are made:

1) When the impact duration is much longer than the time it takes for generated stress waves to travel to the outer boundary of the plate and return, the effects of higher vibrational modes are small and can be neglected. The load deflection behavior of the plate during impact is approximately equivalent to that under a static loading. This type of response, which typically occurs by low velocity impact, is considered to be quasi static in nature (see Rayleigh [9]).

2) The composite laminate behaves like a linear elastic material, so that linear elastic fracture mechanics (LEFM) are applicable to delamination development problems. Consistently with the aforementioned quasi-static approach, the delamination development is supposed to be quasi static, that is, successive stages of static equilibrium are assumed for the energy balance. The delamination growth is dominated by the shearing crack extension mode, that is, it is mainly a matter of mode II crack propagation.

3) The bending deformation in the laminated composite plate is dominant compared with the membrane deformation up to the delamination threshold load. The size of the damage zone is small compared with the size of the plate. The delamination is supposed to only cause a localized disturbance in the deformation field within the impact damage zone. The global deformation of the plate outside the damage zone remains unaffected after the occurrence of the delamination.

4) The damage mechanism transverse matrix cracking occurs to a limited extent, so that the crack area is negligible compared with the delamination area. The damage mechanism fiber breakage is left out of consideration in the current analysis.

5) For simplicity, the analysis is limited to quasi-isotropic laminates in this paper. The delamination that separates the original laminate into two parts can occur along an arbitrary interface within the laminate. Therefore, the delaminated sublaminates may have a general unbalanced unsymmetrical layup. The delamination has an idealized elliptic shape.

B. Bending Energy in Localized Deformation Field

Consider a partially damaged flat plate subjected to the concentrated point load P representing the transverse impact load. The deformation outside the damage zone is modeled with the global deformation field on the basis of the undamaged plate under the load P. The local deformation field inside the damage zone is simulated with two elliptic orthotropic laminates on top of each other under the same P. The major axis of the ellipse is a_0 and the minor axis is b_0. The undamaged area is denoted as A_1 and the delaminated area is A_2 (see Fig. 1).

The classical lamination theory (CLT) is used to describe the constitutive behavior of laminated composites:

$$\begin{Bmatrix} N \\ M \end{Bmatrix} = \begin{bmatrix} A & B \\ B & D \end{bmatrix} \begin{Bmatrix} \epsilon \\ \kappa \end{Bmatrix} \tag{1}$$

The extensional stiffness matrix A relates the in-plane resultant forces N to the midplane strains ϵ of the laminate, whereas the bending stiffness matrix D relates the resultant moments M to the curvatures κ. The bending-extension matrix B describes the coupling between N and κ as well as the coupling between M and ϵ. A partially inverted form of Eq. (1) is

$$\begin{Bmatrix} \epsilon \\ M \end{Bmatrix} = \begin{bmatrix} A^{-1} & -A^{-1}B \\ BA^{-1} & D - BA^{-1}B \end{bmatrix} \begin{Bmatrix} N \\ \kappa \end{Bmatrix} \tag{2}$$

For a pure bending problem with the in-plane forces N equal to zero, the reduced bending stiffness matrix D^* is defined as

$$D^* = D - BA^{-1}B \tag{3}$$

For an infinitesimal element within the undamaged region, the elastic strain energy due to bending per unit area is calculated by the following formula:

$$u(w_1) = \frac{1}{2}\left[D_{11}^* \left(\frac{\partial^2 w_1}{\partial x^2}\right)^2 + 2D_{12}^* \frac{\partial^2 w_1}{\partial x^2}\frac{\partial^2 w_1}{\partial y^2} + D_{22}^* \left(\frac{\partial^2 w_1}{\partial y^2}\right)^2 + 4D_{66}^* \left(\frac{\partial^2 w_1}{\partial x \partial y}\right)^2 \right] \tag{4}$$

where w_1 is the global displacement field in the plate. Similarly, the bending energy per unit area in an infinitesimal element within the delaminated region becomes

$$\tilde{u}(w_2) = \frac{1}{2}\left[\tilde{D}_{11}^* \left(\frac{\partial^2 w_2}{\partial x^2}\right)^2 + 2\tilde{D}_{12}^* \frac{\partial^2 w_2}{\partial x^2}\frac{\partial^2 w_2}{\partial y^2} + \tilde{D}_{22}^* \left(\frac{\partial^2 w_2}{\partial y^2}\right)^2 + 4\tilde{D}_{66}^* \left(\frac{\partial^2 w_2}{\partial x \partial y}\right)^2 \right] \tag{5}$$

where w_2 is the local displacement field in the damage zone due to the weakening of the material. The residual bending stiffness constants $\widetilde{D}_{ij}^*$ can be obtained by summing the corresponding D_{ij}^* components of the delaminated sublaminates. The total bending energy in the plate can be found by integration as follows:

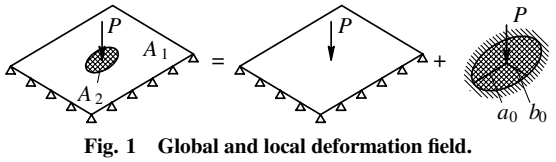

Fig. 1 Global and local deformation field.

$$U = \iint_{A_1} u(w_1)\,\mathrm{d}x\,\mathrm{d}y + \iint_{A_2} \tilde{u}(w_2)\,\mathrm{d}x\,\mathrm{d}y$$
$$= \underbrace{\iint_{A_1+A_2} u(w_1)\,\mathrm{d}x\,\mathrm{d}y}_{\text{constant}} - \iint_{A_2} u(w_1)\,\mathrm{d}x\,\mathrm{d}y + \iint_{A_2} \tilde{u}(w_2)\,\mathrm{d}x\,\mathrm{d}y \tag{6}$$

Equation (6) shows that the bending energy release is, in principle, dependent on both the global field w_1 and the local field w_2. To obtain an upper bound approximation, the term

$$-\iint_{A_2} u(w_1)\,\mathrm{d}x\,\mathrm{d}y + \iint_{A_2} \tilde{u}(w_2)\,\mathrm{d}x\,\mathrm{d}y$$

is calculated by supposing that the plate is entirely clamped outside the elliptic boundary of the damage zone. For the local displacement field w_2, the exact solution $w = w_0[1-(r^2/a_0^2)+2(r^2/a_0^2)\,\ell n(r/a_0)]$ for a clamped isotropic circular plate of radius a_0 loaded at the center in Timoshenko and Woinowsky-Krieger [10] is generalized to the following form in the present study:

$$w_2 = w_0\left[1-\left(\frac{x^2}{a_0^2}+\frac{y^2}{b_0^2}\right)+\left(\frac{x^2}{a_0^2}+\frac{y^2}{b_0^2}\right)\ell n\left(\frac{x^2}{a_0^2}+\frac{y^2}{b_0^2}\right)\right] \tag{7}$$

The expression for w_2 vanishes at the boundary, as does its first derivative; in other words, the boundary conditions imposed by the clamped edge are satisfied. Logically, the maximum displacement w_0 occurs at the loading point, where $\lim_{r\to 0} r^2\,\ell n\, r = 0$ is valid. The bending energy stored in the original laminate within the area A_2 is approximated as follows:

$$\iint_{A_2} u(w_1)\,\mathrm{d}x\,\mathrm{d}y \approx \iint_{A_2} u(w_2')\,\mathrm{d}x\,\mathrm{d}y \tag{8}$$

where the artificial displacement field w_2' corresponds to a clamped undamaged elliptic laminate subjected to a normal load at the center:

$$w_2' = w_0'\left[1-\left(\frac{x^2}{a_0^2}+\frac{y^2}{b_0^2}\right)+\left(\frac{x^2}{a_0^2}+\frac{y^2}{b_0^2}\right)\ell n\left(\frac{x^2}{a_0^2}+\frac{y^2}{b_0^2}\right)\right] \tag{9}$$

By means of the following coordinate transformation:

$$\begin{cases} x = a_0\varrho\cos\vartheta \\ y = b_0\varrho\sin\vartheta \end{cases} \quad \text{with} \quad \left|\frac{\partial(x,y)}{\partial(\rho,\vartheta)}\right| = a_0 b_0 \varrho \tag{10}$$

the total bending energy stored in the plate is found to be

$$U = \text{const} - \frac{8\pi w_0'^2}{a_0 b_0}\bar{D}_0 + \frac{8\pi w_0^2}{a_0 b_0}(\bar{D}_1+\bar{D}_2) \tag{11}$$

The weighted average flexural rigidities $\bar{D}_0$, $\bar{D}_1$, and $\bar{D}_2$ for the original laminate and the first and second delaminated sublaminates are calculated with

$$\bar{D} = \tfrac{1}{8}[3D_{11}^*\lambda^2 + 2(D_{12}^*+2D_{66}^*) + 3D_{22}^*\lambda^{-2}] \tag{12}$$

where λ is the ellipticity ratio of the delamination

$$\lambda = b_0/a_0 \tag{13}$$

The bending stiffness is minimized with respect to the shape of the delamination, so that the potential energy of the system reaches the minimum. This leads to an ellipticity ratio-independent flexural rigidity:

$$\frac{\partial\bar{D}}{\partial\lambda} = 0 \Rightarrow \lambda = \sqrt[4]{\frac{D_{22}^*}{D_{11}^*}} \Rightarrow \bar{D} = \frac{1}{4}(3\sqrt{D_{11}^* D_{22}^*} + D_{12}^* + 2D_{66}^*) \tag{14}$$

Equation (11) can be further simplified by eliminating w_0' and w_0 using the local compliances of the undelaminated and delaminated laminate at the load application point. In doing so, w_0' and w_0 can be replaced by P. The demanded compliances can be calculated from Eq. (11) with the help of the principle of virtual displacement. The local compliance C of the original laminate and the local compliance $\tilde{C}$ of two delaminated sublaminates are, respectively,

$$C = \frac{w_0'}{P} = \frac{a_0 b_0}{16\pi\bar{D}_0} = \frac{A_2}{16\pi^2}\frac{1}{\bar{D}_0}$$
$$\tilde{C} = \frac{w_0}{P} = \frac{a_0 b_0}{16\pi(\bar{D}_1+\bar{D}_2)} = \frac{A_2}{16\pi^2}\frac{1}{\bar{D}_1+\bar{D}_2} \tag{15}$$

Using the compliances obtained, Eq. (11) can be rewritten in the following equivalent form:

$$U = \text{const} - \tfrac{1}{2}P^2 C + \tfrac{1}{2}P^2\tilde{C} \tag{16}$$

C. Energy Balance Analysis Based on Bending

The delamination threshold load can be derived by means of LEFM and, in particular, the Griffith energy criterion [8]. If a crack is in equilibrium, the decrease of strain energy must be equal to the increase of surface energy due to crack extension, that is,

$$G_{\mathrm{II}C} = \frac{\mathrm{d}U}{\mathrm{d}A} \tag{17}$$

where $G_{\mathrm{II}C}$ is the mode II critical energy release rate, which can be measured using the end-loaded split test or the mixed-mode bending test; U is the elastic strain energy in the structure; and A is the crack area. Substituting Eq. (16) into Eq. (17) gives

$$G_{\mathrm{II}C} = \frac{1}{2}P_{\mathrm{cr}}^2\left(\frac{\partial\tilde{C}}{\partial A}-\frac{\partial C}{\partial A}\right) = \frac{P_{\mathrm{cr}}^2}{32\pi^2}\left(\frac{1}{\bar{D}_1+\bar{D}_2}-\frac{1}{\bar{D}_0}\right) \tag{18}$$

where P_{cr} is the delamination threshold load below which a significant delamination will not occur.

To obtain the minimum delamination threshold load that is associated with the maximum potential energy release from the structure, the following minimization problem is formulated:

$$\text{minimize } \xi = \left(\frac{1}{\bar{D}_1+\bar{D}_2}-\frac{1}{\bar{D}_0}\right)^{-1}$$
$$\text{subject to } i = 1,\ldots,N \quad \text{for } 0 \le \theta \le \pi \tag{19}$$

where ξ is the bending stiffness reduction function due to delamination development. The constant N is the number of interfaces and the variable i indicates the location of the delamination, which determines the layup and thickness of the two sublaminates. The minimization problem can be effectively solved using the so-called bracketing method, that is, using a series of function evaluations starting from an initial point. For the discrete variable i, the step size is 1. The angle θ is the orientation of the delamination with respect to the material coordinate system, in which the layup of the laminate is defined. Keeping the ellipse fixed in the x–y coordinate system, the laminate and its sublaminates are rotated with θ during the calculation to achieve the same results. For the continuous variable θ, a sufficiently small step size should be chosen. If the sublaminates possess strong orthotropy, θ is aligned with the fiber direction of the dominant sublaminate.

Having solved the minimization problem, all relevant information about the potential delamination is known. The delamination threshold load then becomes

$$P_{\mathrm{cr}} = \sqrt{32\pi^2 G_{\mathrm{II}C}\xi_{\min}} \tag{20}$$

Using Eq. (20), the delamination threshold load is predicted on the basis of the laminate layup, and the elastic and fracture properties of the lamina. Assuming a midthickness delamination and replacing the two sublaminates with two isotropic layers, Eq. (20) reduces to the equation of Davies and Robinson [6] with $\xi_{\min} = D'/3$, where D' is the isotropic flexural rigidity of the plate. The rigidity D' of an

isotropic plate is proportional to the third power of its thickness. This implies that halving the thickness leads to a reduction of the rigidity with a factor of 8. The residual flexural rigidity of the two delaminated sublaminates is $D'/4$; therefore, $\xi_{\min}$ becomes $D'/3$. It is apparent that the main factor that greatly complicates the problem is the material anisotropy.

As already mentioned, the bending energy release based on elliptic plates with clamped edges leads to an upper bound approximation. Following the same solution procedure, the lower bound of the delamination threshold load can be found by considering elliptic plates with simply supported edges. According to Timoshenko and Woinowsky-Krieger [10], the maximum deflection for a clamped and simply supported isotropic circular plate under a point load P can be expressed as follows:

$$\begin{aligned} w_0 &= \frac{Pa_0^2}{16\pi D} \text{ for a clamped edge} \\ w_0 &= \frac{(3+\nu)Pa_0^2}{16\pi(1+\nu)D} \text{ for a simply supported edge} \end{aligned} \tag{21}$$

where a_0 is the plate radius and ν is Poisson's ratio of the material. For laminates, the ν value can be estimated using the A matrix from the CLT: $\nu = A_{12}/A_{22}$. The scaling factor α between the compliances of a clamped and a simply supported plate is

$$\alpha = (1+\nu)/(3+\nu) \tag{22}$$

Hence, the lower bound of the delamination threshold load can be written as

$$P_{\text{cr}} = \sqrt{32\pi^2 \alpha G_{\text{IIC}} \xi_{\min}} \tag{23}$$

Laminates used in practice usually have an effective ν of about 0.3; the lower bound is then 37% lower compared with the upper bound.

D. Material Degradation Due to Matrix Cracking

As is known, matrix cracks have already occurred before the onset of significant delamination (e.g., see Abrate [1]). The fact that the matrix cracks reduce the transverse modulus of different layers as well as the delamination threshold load can be taken into account by using the progressive damage model proposed by Chang and Lessard [11]. The formation of matrix cracks takes place for the greater part outside the small contact zone, where the highly localized contact stress field has smoothed out. On the basis of Saint-Venant's principle, the matrix cracking mechanism is expected to be dominated by the bending stress field produced by the impact load. For convenience, the residual stresses in the matrix due to the manufacturing processes are neglected.

Because of the $r^2 \ln r$-type singularity, a concentrated point load leads to infinitely large bending moments immediately under the loading point. Hence, the maximum bending moments are calculated on the basis of a simply supported isotropic plate of radius a, for which the load is uniformly distributed over a concentric circular area of radius c ($a \gg c$). The origin of the Cartesian coordinate system x–y coincides with the center of the plate. As demonstrated by Timoshenko and Woinowsky-Krieger [10], the maximum bending moments that occur at the plate center read

$$M_x = M_y = (P_{\text{cr}}/4\pi)\left[(1+\nu)\ln(a/c) + 1\right] \tag{24}$$

The twist moment M_{xy} is equal to 0 at the center, as the plate is symmetrically loaded with respect to the center. In Eq. (24), P_{cr} is the upper bound of the delamination threshold load. The plate radius a corresponds to the shortest distance measured from the impact point to the supporting edges of the global structure. The radius c is taken as equal to the contact radius, which is given by the following expression from Hertz's contact theory [12,13]:

$$c = \sqrt{r_i \alpha} \tag{25}$$

where r_i is the impactor tup radius and the contact indentation α can be solved through Hertz's law [14]:

$$P_{\text{cr}} = n\alpha^{\frac{3}{2}} \quad \text{with} \quad n \approx \tfrac{4}{3} r_i^{\frac{1}{2}} E_2 \tag{26}$$

where E_2 is the elastic modulus transverse to the fiber direction.

With the prescribed maximum moments $M = \{M_x, M_y, 0\}^T$, the maximum middle surface curvatures due to bending $\kappa = \{\kappa_x, \kappa_y, \kappa_{xy}\}^T$ then become:

$$\kappa = D^{-1} M \tag{27}$$

where D is the bending stiffness matrix of the original laminate. For an arbitrary kth layer, the stresses in the principal material directions $\sigma_k = \{\sigma_1, \sigma_2, \tau_{12}\}_k^T$ are

$$\sigma_k = zT\bar{Q}_k\kappa \tag{28}$$

where z is the distance from the middle surface of the laminate, T is the transformation matrix between the x–y coordinates and the principal material coordinates, and $\bar{Q}_k$ is the transformed reduced stiffness matrix of the kth layer. In Eq. (28), T and $\bar{Q}_k$ are calculated in accordance with the CLT [8].

By reason of the symmetric layup, the geometrical middle surface of a quasi-isotropic laminate acts as the neutral surface of bending. The layers below the neutral surface are expected to fail by matrix tensile cracking when the maximum stresses in the layers satisfy the following failure criterion [11]:

$$(\sigma_2/Y_t)^2 + (\tau_{12}/S_{12})^2 = 1 \tag{29}$$

where Y_t is the transverse tensile strength and S_{12} is the shear strength of the lamina. For matrix compression failure in the layers above the neutral surface, the following failure criterion [11] applies

$$(\sigma_2/Y_c)^2 + (\tau_{12}/S_{12})^2 = 1 \tag{30}$$

where Y_c is the transverse compression strength of the lamina. On the basis of the stresses obtained from Eq. (28), it can be predicted whether the matrix cracks have occurred in a certain layer. If so, the transverse Young's modulus E_2 is reduced to 0 in that layer:

$$E_2 = 0 \tag{31}$$

whereas the longitudinal Young's modulus E_1, the in-plane shear modulus G_{12}, and Poisson's ratios ν_{12} and ν_{21} remain constant throughout the damage development process. Then the bending stiffness constants $\bar{D}_0$, $\bar{D}_1$, and $\bar{D}_2$ can be calculated once again by means of the CLT, ending in decreased upper and lower bounds for the delamination threshold load.

To summarize, a damage mechanics idea has been incorporated into the fracture-mechanics-based delamination initiation model to include the effects of matrix cracking. In contrast to the preceding paragraphs, the delamination threshold load here becomes dependent on the global structural size, the boundary conditions, the impactor target contact, the strength properties of the laminae, etc. For this reason, it can not be taken for granted that the impact test results obtained with extracted small laboratory specimens always apply to a full-scale structure. This illustrates the importance of developing an analytical model to predict the behavior of a composite structure on the basis of fundamental material properties.

III. Modeling Delamination Growth

This section takes a step forward to derive an analytical solution for the growth of significant delaminations. Again, the modeling is based on the LEFM approach, whereas some new assumptions have to be made to achieve realistic results, especially the effects that are connected with multiple delaminations.

A. Geometry of Idealized Multiple Delaminations

It has been empirically observed that impact-induced damage consists frequently of matrix cracks and multiple delaminations. Accordingly, the modeling of delamination growth may not rely on a single delamination. As displayed in Fig. 2, the current study assumes idealized multiple delaminations, of which the individual delaminations are elliptic. The area of the ith delamination is A_i and the total number of the delaminations is n. The external contour of the damage zone is circular, and its area is S. In the analysis, this contour is actually the boundary of the localized deformation field.

Assuming that the major axes of the ellipses are equal to the radius of the circle, the total actual crack area and the damage area are related to each other by the following equation:

$$\sum_{i=1}^{n} A_i = S \sum_{i=1}^{n} \lambda_i \tag{32}$$

For later validation work, it is convenient to introduce the projected area of the delaminations, which is detectable using an ultrasonic C scan. The projected area of the delaminations A_p is calculated by subtracting the overlapping area from the total crack area:

$$A_p \approx S\left[\sum_{i=1}^{n} \lambda_i - (n-1)\left(\frac{\sum_{i=1}^{n} \lambda_i}{n}\right)^2\right] \tag{33}$$

where the overlapping area is estimated using the average radius of the interior tangent circles of the ellipses. For a large number of delaminations or ellipticity ratios close to 1, the following equation is a reasonable approximation:

$$A_p \approx S \tag{34}$$

The last area definition that needs to be introduced is S':

$$S' \approx \frac{1}{4}\left(\frac{\sum_{i=1}^{n} \lambda_i}{n} + 1\right)^2 S \tag{35}$$

The area S' is based on a circle with its radius equal to the average of all major and minor axes of the ellipses. This effective area will be used to describe the size of the damage zone in the global buckling analysis, in which the damage zone is simplified to n circular delaminations. The reason for this simplification is that the global deformation field is dominant when the plate is loaded under a uniform in-plane compression.

B. Stability of Delamination Propagation

Using Eq. (32), Eq. (20) for the delamination threshold load can be generalized in the following form suitable for the multiple delaminations:

$$P_n = \sqrt{\frac{32\pi^2 G_{\mathrm{IIC}} \sum_{i=1}^{n} \lambda_i}{(\sum_{i=1}^{n+1} \bar{D}_i)^{-1} - \bar{D}_0^{-1}}} \tag{36}$$

where the ellipticity ratio λ_i for the ith delamination can be approximated on the basis of the anisotropic properties of two adjacent sublaminates:

$$\lambda_i = \sqrt[4]{\frac{D^*_{22,i} + D^*_{22,i+1}}{D^*_{11,i} + D^*_{11,i+1}}} \tag{37}$$

For the special case $n = 1, \lambda_1 = 1$ holds. P_n for $n = 1, 2, 3, \cdots$ can be interpreted as the critical load at which n delaminations along the given interfaces will start to grow. If the material anisotropy is neglected, Eq. (36) reduces to the equation of Olsson et al. [7] for the threshold load of n delaminations. That means that the term

$$\sum_{i=1}^{n} \lambda_i$$

increases with the order $\mathcal{O}(n)$. The n delaminations separate the laminate into $n + 1$ sublaminates of equal thickness, and the flexural rigidity of each sublaminate is reduced to $1/(n+1)^3$ compared with the original laminate. This implies that the total residual flexural rigidity

$$\min\left(\sum_{i=1}^{n+1} \bar{D}_i\right)$$

is of the order $\mathcal{O}[1/(n+1)^2]$. After some simplifications, P_n is found to decrease with an increasing n with the order $\mathcal{O}[1/\sqrt{n+2}]$.

Hypothetically speaking, if there is a single delamination throughout the entire process, the delamination starts to grow without further load increase when the delamination threshold load is exceeded. In the case of multiple delaminations, the load defection curve will decrease in a stepwise pattern, resulting in an unstable crack propagation, as the energy released is larger than the energy required for growth. However, the reality is that the maximum impact load is in most cases higher than the delamination threshold load. This implies that a mechanism should exist that leads to a stable crack growth. For clarity, a load deflection curve is shown in Fig. 3, in which the impact load P is plotted against the deflection δ under the loading point. The topic of the identification of the underlying mechanism will be dealt with in Sec. III.C.

C. Energy Balance Based on Membrane Deformation

Unlike the delamination initiation model, a proper modeling of the delamination propagation means that the membrane strain energy within the damage zone due solely to the stretching of the middle surface has to be taken into account. It can be expected that the membrane effects become significant in that region when the bending stiffness has been dramatically reduced and the membrane stiffness remains unchanged, as the load-carrying fibers preserve their properties and orientations. This implies that Eq. (18) for the energy release needs to be updated by adding an extra membrane term.

The linearized stiffness of the membrane can be derived from the large deflection solution for an isotropic circular plate under a point load P (see Timoshenko and Woinowsky-Krieger [10]):

$$\frac{w_0}{h} + c_1\left(\frac{w_0}{h}\right)^3 = c_2 \frac{P a_0^2}{\tilde{E} h^4} \tag{38}$$

where w_0 is the maximum deflection of the circular plate, h is the plate thickness, and a_0 is the plate radius. The constants c_1 and c_2 are dependent on the boundary conditions. If the plate is clamped at the edge, c_1 is equal to 0.200 and c_2 is equal to 0.217. If the plate is

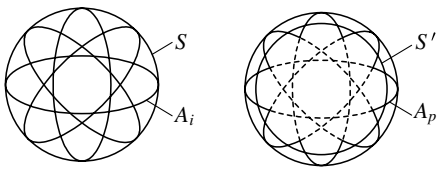

Fig. 2 Idealized multiple delaminations.

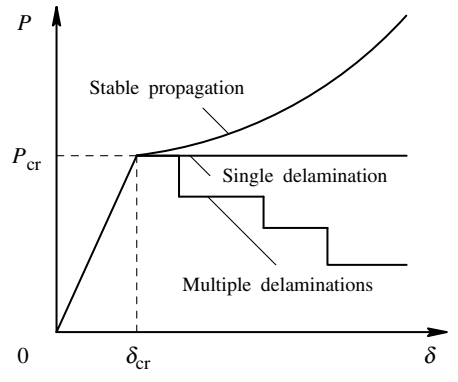

Fig. 3 Stable and unstable delamination growth.

simply supported, c_1 is equal to 0.272 and c_2 is equal to 0.552. The effective engineering elastic modulus $\tilde{E}$ of the delaminated sublaminates is taken as equal to the effective modulus of the original laminate:

$$\tilde{E} = (1/h)\left[A_{11} - \left(A_{12}^2/A_{22}\right)\right] \tag{39}$$

where A_{ij} are components of the A matrix. Differentiating Eq. (38) with regard to w_0, Eq. (15) describing the total residual stiffness of the delaminated sublaminates with clamped edges can be rewritten as:

$$\frac{1}{\tilde{C}} = \frac{16\pi^2}{S}\left(\sum_{i=1}^{n+1}\bar{D}_i + \frac{1}{18}\tilde{E}hw_0^2\right) \tag{40}$$

The global deformation of the plate is still assumed to have a character of pure bending; therefore, Eq. (15) for the original stiffness of the undamaged plate remains valid. On the basis of Eq. (40), the linearized energy balance including the membrane deformation within the damage zone can now be expressed as follows:

$$P_p = \sqrt{\frac{32\pi^2 G_{\mathrm{IIC}}\sum_{i=1}^{n}\lambda_i}{(\sum_{i=1}^{n+1}\bar{D}_i + \frac{1}{18}\tilde{E}hw_0^2)^{-1} - \bar{D}_0^{-1}}} \tag{41}$$

The term

$$G_{\mathrm{IIC}}\sum_{i=1}^{n}\lambda_i$$

can be considered a resultant critical energy release rate for multiple delaminations:

$$G_C = G_{\mathrm{IIC}}\sum_{i=1}^{n}\lambda_i \tag{42}$$

When the laminate bending stiffness is significantly reduced by multiple delaminations, it is apparent that the damage zone starts to behave more like a flexible membrane, that is,

$$\left(\sum_{i=1}^{n+1}\bar{D}_i + \frac{1}{18}\tilde{E}hw_0^2\right)^{-1} \gg \bar{D}_0^{-1}$$

and

$$\sum_{i=1}^{n+1}\bar{D}_i \ll \frac{1}{18}\tilde{E}hw_0^2$$

After neglecting the two aforementioned terms, Eq. (41) can be reduced to the following linear equation:

$$P_p = \frac{4\pi w_0}{3}\sqrt{\tilde{E}hG_C} \tag{43}$$

Analogously to the lower bound of the delamination threshold load, a similar equation for the delamination propagation can be derived for a simply supported edge:

$$P_p = \frac{4\pi w_0}{\sqrt{17}}\sqrt{\tilde{E}hG_C} \tag{44}$$

where

$$\tilde{C}^{-1} = \frac{16\pi^2}{S}\left(\frac{1+\nu}{3+\nu}\sum_{i=1}^{n+1}\bar{D}_i + \frac{1}{34}\tilde{E}hw_0^2\right)$$

Then the delamination propagation curve starting from the delamination threshold load can be expressed as follows:

$$P - P_{\mathrm{cr}} = \frac{\delta - \delta_{\mathrm{cr}}}{C_p} \quad \text{with} \quad C_p = C_u + (\beta\sqrt{\tilde{E}hG_C})^{-1} \tag{45}$$

The compliance C_p of the delamination propagation curve is the sum of the undamaged structural compliance C_u and the apparent compliance of the enlarging membrane. The constant β is equal to

$$\begin{aligned} &\beta = 4\pi/3 \text{ for the clamped edge} \\ &\beta = 4\pi/\sqrt{17} \text{ for the simply supported edge} \end{aligned} \tag{46}$$

This means that the lower bound for the delamination propagation is about 27% lower compared with the upper bound. Using the present analysis, the load applied is found to be by approximation proportional to the maximum deflection of the membrane when the energy balance for delamination propagation is satisfied. The load defection curve from the impact test may manifest an almost linear increase after the delamination threshold load. This increase arises from the membrane deformation, which lowers the energy release within the damage zone.

D. Determination of Resultant Critical Energy Release Rate

Similarly to the preceding single delamination case, P_p has to be minimized with respect to the distribution of multiple delaminations so that the resultant critical energy release rate G_C can be determined:

$$\begin{aligned} &\text{minimize} \quad \Lambda = \frac{1}{\bar{D}_0}\left(\sum_{i=1}^{n+1}\bar{D}_i + \frac{1}{18}\tilde{E}hw_0^2\right)\left(\sum_{i=1}^{n}\lambda_i\right) \\ &\text{subject to } n = 1,\ldots,N \quad \text{for } 0 \le \theta \le \pi \end{aligned} \tag{47}$$

This minimization problem is formulated on the basis of Eq. (41). The integer variable n is the number of delaminations and N is the number of interfaces. The angle θ is the orientation of the multiple delaminations in reference to the material coordinate system. For the sake of simplicity, the individual delaminations are assumed to have a fixed orientation with respect to each other, that is, the mutual orientation is determined by the laminate layup. The deflection w_0 can be roughly estimated using Eq. (38), in which the flexural rigidity is modified to

$$\sum_{i=1}^{n+1}\bar{D}_i$$

The load P is taken as equal to the delamination threshold load P_{cr}, and the radius of the delaminated plate is chosen to reflect a realistic range of the damage size. The stiffness constant $\bar{D}_0$ is used as a weighting factor to make the parameter Λ dimensionless and, therefore, does not influence the final results.

The minimization of Λ can be performed using the same procedure as in the case of the threshold load calculation. Physically, the minimization process means the determination of the condition of how the energy balance can be most easily satisfied. Keeping the deflection w_0 constant, it can be verified that the term

$$\sum_{i=1}^{n+1}\bar{D}_i\sum_{i=1}^{n}\lambda_i$$

in the target function Λ decreases frequently with an increasing number of delaminations, and the term

$$\frac{1}{18}\tilde{E}hw_0^2\sum_{i=1}^{n}\lambda_i$$

is commonly monotonically increasing. On the one hand, the system strives for the maximum bending energy release and has a tendency to create as many delaminations as possible. On the other hand, the total crack area increases with increasing amount of delaminations, resulting in a higher resultant critical energy release rate and, therefore, a larger crack resistance. The interaction between these two effects leads to a U-shaped Λ curve, which first decreases and then increases. The minimum Λ represents the most energetically favorable combination of the bending energy release and the crack area. Through the minimization, the final amount of the delaminations and their location and shape are solved, from which the resultant critical energy release rate G_C and other relevant

parameters follow. The major advantage of the current energy-based approach is that the complex impact process, in which more cracks are successively initiated and subsequently interact with each other, does not need to be followed step by step. This simplifies the problem to a great extent.

To get an impression of the computational effort, the total number of possible locations of delaminations for N interfaces can be determined by summing the binomial coefficients:

$$\sum_{n=1}^{N}\binom{N}{n} = 2^N - 1$$

For a large number of interfaces, a more efficient minimization algorithm is desirable; however, this topic is beyond the scope of the current study.

IV. Area of Impact-Induced Damage

Usually, the impact energy is used to describe the intensity of an impact event, whereas the resulting damage area is used to indicate the damage resistance. The analytical solutions obtained for the delamination initiation and propagation are actually based on an instantaneous energy balance, in which the crack area has been eliminated for simplification. When considering the energy balance for the entire process, the relationship between the damage area and the impact energy or the peak impact load can be derived.

A. Simplified Load Deflection Curve

Based on the already presented analytical solutions, a simplified load deflection curve is constructed in Fig. 4. The first straight line of the bilinear loading curve represents a linear elastic bending deformation of the undamaged plate, whereas the second straight line represents the linearized delamination propagation curve based on the localized deformation field in the damage zone. The knee point is the delamination initiation point, which corresponds with the delamination threshold load. For the sake of convenience, the unloading curve is supposed to be linear and parallel to the loading curve before the knee point. This simplification comes down to the neglect of the elastic deformation energy stored in the damaged part compared with the undamaged part of the plate. The rebound deformation of the damage zone is then, in a manner of speaking, frozen during the unloading, so that the rebound stiffness can be approximated by the deformation of the undamaged plate. For the same reason, the unloading curve does not return to the origin of the graph.

B. Relationship Damage Area and Peak Impact Load

Assuming that the plate deflection δ is equal to the impactor displacement, the gravitational force is negligible, and the impactor velocity is 0 at the maximum deflection, the work done by the contact force along the loading curve is equal to the impact energy, which is basically the initial kinetic energy of the impactor. The work done by the contact force along the unloading curve is equal to the impactor kinetic energy at the end of the impact event. Briefly, the impact energy E is the area under the loading curve, whereas the impactor energy loss ΔE is the area enclosed by the complete load deflection curve:

$$E = \int_0^{\delta_{\max}} P\,\mathrm{d}\delta, \qquad \Delta E = \int_0^{\delta_{\text{end}}} P\,\mathrm{d}\delta \tag{48}$$

In accordance with the simplified load deflection curve as shown in Fig. 4, the integrals in Eqs. (48) can be replaced by the following equations:

$$\begin{aligned} E &= \tfrac{1}{2}P_{\text{cr}}\delta_{\text{cr}} + \tfrac{1}{2}(P_{\max} + P_{\text{cr}})(\delta_{\max} - \delta_{\text{cr}}) \\ \Delta E &= E - \tfrac{1}{2}P_{\text{cr}}\delta_{\text{cr}}\left(\frac{P_{\max}}{P_{\text{cr}}}\right)^2 \end{aligned} \tag{49}$$

The compliance of the undamaged plate C_u and the compliance of the delamination propagation curve C_p are

$$C_u = \frac{\delta_{\text{cr}}}{P_{\text{cr}}}, \qquad C_p = \frac{\delta_{\max} - \delta_{\text{cr}}}{P_{\max} - P_{\text{cr}}} \tag{50}$$

Logically, the delamination threshold energy E_{cr} is defined by

$$E_{\text{cr}} = \tfrac{1}{2}P_{\text{cr}}\delta_{\text{cr}} \tag{51}$$

Using Eqs. (49) and (50), the impactor energy loss is expressed as a parabolic function of the peak impact load:

$$\Delta E = \tfrac{1}{2}(C_p - C_u)\left(P_{\max}^2 - P_{\text{cr}}^2\right) \tag{52}$$

According to the law of conservation of energy, the loss of the impactor kinetic energy is equal to the energy absorbed due to damage development, if the small amount of heat energy due to plastic deformation, sound energy, etc., is neglected. Because the greatest part of the dissipated fracture energy is consumed for the formation of multiple delaminations, the following relationship between the impactor energy loss and the damage area is valid:

$$\Delta E = G_C S \tag{53}$$

Substituting Eq. (53) into Eq. (52), the damage area becomes

$$S = \frac{P_{\max}^2 - P_{\text{cr}}^2}{2\beta\sqrt{\tilde{E}hG_C^3}} \tag{54}$$

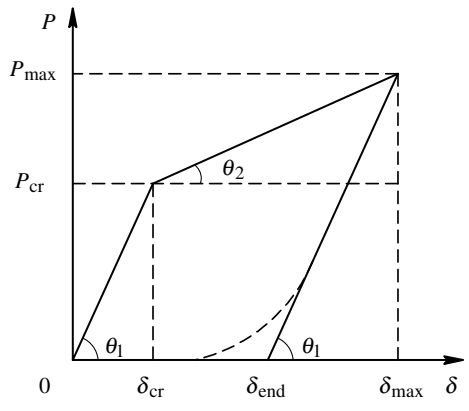

Fig. 4 Simplified load deflection curve.

C. Relationship Damage Area and Impact Energy

With the help of Eqs. (50), directly eliminating the variables $P_{\max}$ and $\delta_{\max}$ from Eqs. (49) yields

$$\Delta E = H(E - E_{\text{cr}})(E - E_{\text{cr}})[1 - (C_u/C_p)] \tag{55}$$

where $H(E - E_{\text{cr}})$ is the Heaviside step function indicating that ΔE is equal to 0 for $E \le E_{\text{cr}}$. On the basis of the last term appearing in Eq. (55), a parameter can be introduced as the impact energy transfer factor:

$$\Gamma = 1 - (C_u/C_p) \tag{56}$$

The minimum energy transfer factor $\Gamma = 0$ corresponds to an complete restitution of the elastic energy when no damage development takes place. The maximum energy transfer $\Gamma = 1$ corresponds to an unstable delamination growth, resulting in the highest possible energy dissipation. Using Eq. (56), Eq. (55) can be rewritten as:

$$S = (\Gamma/G_C)H(E - E_{\text{cr}})(E - E_{\text{cr}}) \tag{57}$$

Equation (57) shows that the damage area is linearly related to the impact energy. It is clear that the impact damage resistance can be

improved not only by increasing the fracture toughness G_{IIC} of the material, but also by optimizing the layup of the laminate and the stiffness of the structure, which plays an important role in the energy transfer from the impactor to the target.

Up to this point, the equations for the impact behavior of composite structures have been derived. Compared with the aforementioned reviews [1–5], it is clear that all important experimental parameters affecting the impact resistance characteristics have been incorporated into the analytical model in a logical way, for example, lamina stiffness and strength, fracture toughness, laminate thickness, stacking sequence, etc. The model can be used in impact resistance analyses either in a deterministic or probabilistic manner. If the extrinsic variables such as the impactor kinetic energy, the impactor radius, and stiffness are considered probabilistic in nature because of the uncertainty of the in-service environment, the current model can be readily used in Monte Carlo simulations, as the computational effort required by a large number of random trials is still limited.

V. Damage Tolerance Analysis

When the damaged plate is loaded under compression, the impact-induced delaminations may significantly reduce the global bending stiffness of the plate, resulting in a decrease in the critical global buckling load and the accompanying postbuckling strength. Recall the plate containing a circular damage zone: the out-of-plane impact loading is replaced by uniform in-plane compression in two perpendicular directions (see Fig. 5). In the current study, the residual compression strength analysis of the plate is limited to the global buckling mode. The local failure mode termed delamination buckling, in which delaminated sublaminates buckle locally at first, followed by a stable or an unstable delamination growth until the plate finally fails, is left out of consideration. Using sophisticated finite element techniques, Remmers and de Borst [15] demonstrated that the membrane energy release due to a locally buckled sublaminate is limited and the delamination propagation begins at a very high stress level far beyond what can be expected in engineering practice.

In the buckling analysis, the plate is assumed to buckle slightly under the action of the midplane forces, and the critical buckling loads are obtained by calculating the magnitudes that the forces must have to keep the plate in the slightly buckled shape. From the energetic point of view, it is equivalent to compare the strain energy of bending with the corresponding work done by the midplane forces. If the work done by these forces is larger than the bending energy for every possible shape of lateral deflection, the equilibrium state becomes unstable and buckling occurs (see Timoshenko and Gere [16]).

The variation in the lateral displacement δw is described with a double-sine function from Navier's solution for simply supported rectangular plates:

$$\delta w = a_{mn} \sin(m\pi x/a) \sin(n\pi y/b) \tag{58}$$

In the membrane prebuckling state, w is still equal to 0 and δw is the infinitely small buckle displacement. The integers m and n are the number of buckle half-wavelengths in the x and y directions, respectively. The work of the forces N_x, N_y, and N_{xy} acting in the midplane of the plate reads

$$\Delta T = \frac{1}{2} \iint_{S_1+S_2} \left[N_x \left(\frac{\partial w}{\partial x}\right)^2 + N_y \left(\frac{\partial w}{\partial y}\right)^2 + 2N_{xy} \frac{\partial w}{\partial x} \frac{\partial w}{\partial y} \right] \mathrm{d}x\, \mathrm{d}y \tag{59}$$

When the plate is compressed in two directions, N_{xy} vanishes. Without losing generality, N_y is supposed to be equal to ψN_x, where ψ is an arbitrary constant. Then ΔT becomes

$$\Delta T = \frac{\pi^2 abN_x a_{mn}^2}{8} \left(\frac{m^2}{a^2} + \psi \frac{n^2}{b^2} \right) \tag{60}$$

Analogous to Eq. (6), the strain energy of bending is computed using an area integral encompassing the entire domain of the plate:

$$\Delta U = \iint_{S_1} u(\delta w)\, \mathrm{d}x\, \mathrm{d}y + \iint_{S_2} \tilde{u}(\delta w)\, \mathrm{d}x\, \mathrm{d}y \tag{61}$$

The critical buckling load follows from

$$\Delta T = \Delta U \tag{62}$$

The critical buckling stress σ_{cr} for the undamaged plate presented by Whitney [8] can then be obtained:

$$\sigma_{cr} = \frac{\pi^2 \Omega}{h} \left(\frac{m^2}{a^2} + \psi \frac{n^2}{b^2} \right)^{-1} \tag{63}$$

where ψ is equal to ν_{xy} due to the Poisson effect if the edges at $y = 0$ and $y = b$ are immovable in the y direction. When the plate is compressed only in the x direction, ψ is equal to 0. The constant Ω depends on the bending stiffness components, the buckling mode, and the dimension of the plate. Using the reduced bending stiffness method, an unsymmetrically laminated plate can be treated as an orthotropic plate. For quasi-isotropic laminates, the relation $D_{ij}^* = D_{ij}$ is valid, and Ω can be calculated using

$$\Omega = D_{11} \frac{m^4}{a^4} + 2(D_{12} + 2D_{66}) \frac{m^2 n^2}{a^2 b^2} + D_{22} \frac{n^4}{b^4} \tag{64}$$

Taking the critical buckling stress for the undamaged plate as a reference, the critical buckling stress $\tilde{\sigma}_{cr}$ of a damaged plate is normalized as follows:

$$\zeta = \tilde{\sigma}_{cr} / \sigma_{cr} \tag{65}$$

The energy equation (62) implies that the critical buckling load is proportional to the bending energy stored in the plate. The relative decrease of the critical buckling load due to the presence of impact damage is equivalent to the relative decrease of the bending energy of the plate. Thus, the normalized critical buckling load ζ is equal to the bending energy reduction ratio:

$$\begin{aligned} \zeta &= \frac{\iint_{S_1} u(\delta w)\, \mathrm{d}x\, \mathrm{d}y + \iint_{S_2} \tilde{u}(\delta w) \mathrm{d}x\, \mathrm{d}y}{\iint_{S_1+S_2} u(\delta w)\, \mathrm{d}x\, \mathrm{d}y} \\ &= 1 - \frac{\iint_{S_2} [u(\delta w) - \tilde{u}(\delta w)]\, \mathrm{d}x\, \mathrm{d}y}{\iint_{S_1+S_2} u(\delta w)\, \mathrm{d}x\, \mathrm{d}y} \end{aligned} \tag{66}$$

For an undamaged infinitesimal element, the bending energy based on the displacement field in Eq. (58) is

$$u(\delta w) \approx \frac{\pi^4}{2} \Omega a_{mn}^2 \left(\sin \frac{m\pi x}{a} \sin \frac{n\pi y}{b} \right)^2 \tag{67}$$

This equation is an approximate equation, as the term $\pi^4 D_{66} \frac{m^2 n^2}{a^2 b^2} (\cos \frac{2m\pi x}{a} + \cos \frac{2n\pi y}{b})$ has been neglected to simplify the analysis. The neglected term is generally small in comparison to the retained term. The integral of the neglected term over the entire

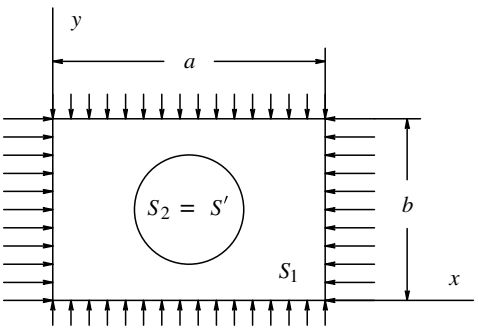

Fig. 5 Simply supported rectangular plate under compression.

rectangular surface is equal to 0. For the bending energy $\tilde{u}(\delta w)$ in a damaged infinitesimal element, Ω is replaced by $\tilde{\Omega}$:

$$\tilde{\Omega} = \tilde{D}_{11}^* \frac{m^4}{a^4} + 2(\tilde{D}_{12}^* + 2\tilde{D}_{66}^*) \frac{m^2 n^2}{a^2 b^2} + \tilde{D}_{22}^* \frac{n^4}{b^4} \tag{68}$$

where the resultant reduced bending stiffness matrix is given by

$$[\tilde{D}^*] = \sum_{i=1}^{n} [\tilde{D}_i^*] \tag{69}$$

Observing that

$$\int_0^b \int_0^a \left(\sin \frac{m\pi x}{a} \sin \frac{n\pi y}{b} \right)^2 \mathrm{d}x\, \mathrm{d}y = \frac{ab}{4}$$

the normalized critical buckling load can be rewritten as

$$\zeta = 1 - \left(1 - \frac{\tilde{\Omega}}{\Omega}\right) \frac{4}{ab} \iint_{S'} \left(\sin \frac{m\pi x}{a} \sin \frac{n\pi y}{b} \right)^2 \mathrm{d}x\, \mathrm{d}y \tag{70}$$

For the sake of convenience, the integral over the circular area S' in Eq. (70) is evaluated using numerical integration on the basis of Simpson's rule, in which the numerical error is kept below 10^{-6}. The integration over a square domain with its area equal to S' forms a rough approximation.

A rectangular flat plate has a stable equilibrium path after buckling. In the buckled state, the plate is still capable of carrying additional load. However, the stress in the plate is no longer uniformly distributed and the central part of the plate is less heavily loaded compared with the parts close to the supported edges. If the plate fails after buckling, the material compression failure strength σ_m should be higher than the critical buckling σ_{cr}. According to the von Kármán postbuckling strength theory, the ultimate strength of the buckled plate is equal to (see Brush and Almroth [17]):

$$\sigma_{\mathrm{ult}} = \sqrt{\sigma_{\mathrm{cr}} \sigma_m} \quad \text{for } \sigma_m \geq \sigma_{\mathrm{cr}} \tag{71}$$

Finally, the remaining ultimate compression strength $\tilde{\sigma}_{\mathrm{ult}}$ of a damaged plate can be expressed in the following form:

$$\tilde{\sigma}_{\mathrm{ult}} = \sqrt{\zeta \sigma_{\mathrm{cr}} \sigma_m} \quad \text{for } \sigma_m \geq \sigma_{\mathrm{cr}} \tag{72}$$

Up to now, all equations are available, which make it possible to calculate the residual strength from the impact energy. This completes the derivation of the analytical solutions for the impact damage resistance and tolerance of laminated composite plates.

VI. Verification and Comparisons

For the purpose of verifying the theoretical work, a series of experiments is conducted in conformance with the standard impact and compression-after-impact (CAI) testing method as specified in BSS-7260 [18]. The prediction accuracy of the analytical solutions can then be determined on the basis of the correlation with the experimental results obtained. For the sake of brevity, the experiments are described in broad outlines here; detailed information can be found in Huang [19].

A. Experiments

The impact tests are performed by means of a Dynatup 8250 instrumented drop weight impact machine. The impactor mass is 3.035 kg and the diameter of the semispherical impactor nose is 20 mm. The nominal impact energy varies from 5 to 30 J. The extent of impact damage is measured using an ultrasonic C scan. The CAI tests are carried out with a Schenck 250 kN screw-driven tensile testing machine. The compression speed is 0.1 mm/min. The standard impact test fixture with a window of 125×75 mm and the standard CAI test fixture are shown in Fig. 6. The specimens are prepared from two different kinds of commercial unidirectional thermoplastic prepregs, carbon fiber (T300) reinforced polyetherimide (PEI) and carbon fiber (AS4) reinforced polyetheretherketone

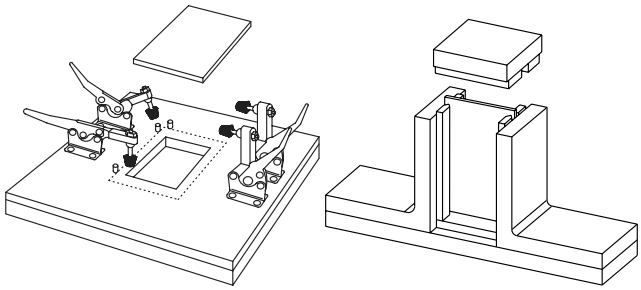

Fig. 6 Standard impact and CAI test fixture.

(PEEK), which is designated aromatic polymer composite (APC-2). The T300/PEI specimens have a $[45_4, 0_4, -45_4, 90_4]_s$ layup and the external dimensions are $152.4 \times 101.6 \times 4.64$ mm. The APC-2 specimens have a $[45_5, 0_5, -45_5, 90_5]_s$ layup and the external dimensions are $152.4 \times 101.6 \times 5.20$ mm.

The load history recorded shows that the duration of an impact event often lies in the order of several milliseconds. The impact load increases from 0 to the peak value during the deformation portion of the impact and decreases back again to 0 during the restoration period. Neglecting the contact indentation, the plate deflection δ at time t is taken as equal to the impactor displacement, which can be calculated by means of the following convolution integral:

$$\delta(t) = v_0 t - \frac{1}{m} \int_0^t P(\tau)(t - \tau)\, \mathrm{d}\tau \tag{73}$$

where m is the impactor mass and v_0 is the initial velocity of the impactor just before impact. Equation (73) expresses the impactor response to the force P in the form of a superposition of impulse responses. Through twice differentiation with respect to time t, it is clear that Eq. (73) is equivalent to Newton's second law. The load deflection curves are then obtained by plotting the measured load signal $P(t)$ against the calculated deflection signal $\delta(t)$. To facilitate the comparison, the experimental graphs are discussed along with the analytical results in later paragraphs (see also Appendix B).

When the impact energy is higher than 15–20 J, fiber breakages are clearly perceptible from the specimen surface. For lower energy levels, matrix cracks occur on a limited scale; the damage is barely visible except for a permanent contact indentation. The ultrasonic C-scan results reveal that all specimens contain an approximately circular damage zone that consists mainly of delaminations. Through the microscopic study of the cross sections of the damage zone, it is observed that large delaminations are frequently located along the $-45/90$ and $90/-45$ interfaces.

From the compression tests, it turns out that the impacted specimens fail through the middle, where the damage zone is located. The nonimpacted specimens fail at the top clamp edge. In all cases, the in-plane load deflection curves go linearly up until the catastrophic failure occurs. The maximum compressive load decreases with the increasing impact energy level. Using a laser measurement, it is observed that the final failure is related to the global buckling of the plates and the delamination buckling mechanism does not play a part in the tests.

B. Delamination Initiation

The laminate layup notation $[45_n, 0_n, -45_n, 90_n]_s$ is, in fact, meant for manufacturing purposes; for the analyses, the simplified layup $[45, 0, -45, 90]_s$ is used with a modified ply thickness. The analytical model predicts that a delamination closer to the midplane leads to more bending stiffness reduction, and the maximum is found at the $-45/90$ interface. As there is no mechanical property mismatch between two adjoining 90–90 layers, the 90/90 interface is not a true interface for crack formation (see Table 1). Using the isotropic approximation based on the midthickness delamination, the bending stiffness of the delaminated sublaminates is overestimated to a large extent, as the anisotropy-related coupling effects are omitted. The

Table 1 Bending stiffness reduction without matrix cracking

i	Sublaminates	Λ for T300/PEI	Λ for APC-2
1	$[45], [0, -45, 90_2, -45, 0, 45]$	0.53	0.55
2	$[45,0], [-45, 90_2, -45, 0, 45]$	0.27	0.29
3	$[45, 0, -45], [90_2, -45, 0, 45]$	0.13	0.15
——	Isotropic approximation	0.25	0.25

Table 2 Comparison of delamination threshold loads in kilonewtons

T300/PEI				
Experimental	Analytical	Lower	Upper	Average
	Current model[a]	2.4	3.8	3.1
2.7	Current model[b]	3.5	5.5	4.5
	Isotropic model[b]	5.3	8.4	6.8
APC-2				
Experimental	Analytical	Lower	Upper	Average
	Current model[a]	4.1	6.5	5.3
4.8	Current model[b]	4.7	7.4	6.0
	Isotropic model[b]	6.5	10.3	8.4

[a]Matrix cracking taken into account.
[b]Matrix cracking left out of consideration.

material properties needed for the calculations are given in Appendix A.

The theoretical delamination threshold loads in the form of the lower and upper bounds are presented in Table 2. The experimental delamination threshold loads are determined on the basis of the load deflection curves in Fig. 7. The onset of large-scale delamination growth manifests itself in the sudden change of the structural stiffness; therefore, the delamination threshold loads correspond with the knee points in the load deflection curves. As expected, the predictions allowing for the effects of material anisotropy and property degradation due to matrix cracking show the best agreement with the measurements. Other predictions, by neglecting these effects, overestimate the delamination threshold loads to a different degree. With regard to the material properties, APC-2 has a higher transverse strength and fracture toughness than T300/PEI and is therefore less susceptible to matrix cracking and delamination. Also, a slightly larger thickness of APC-2 laminates contributes to their better impact resistance compared with T300/PEI laminates. Through comparison, it is further found that the experimental values can be predicted by averaging the theoretical lower and upper bounds. The accuracy achieved for T300/PEI and APC-2 laminates is 88.1 and 90.9%, respectively. In later calculations, the average values are used when the delamination threshold loads are demanded. For a conservative prediction, the lower bound is still recommended.

C. Delamination Growth

The prediction of the bilinear load deflection curves, particularly the delamination propagation curves, requires solving the minimization problem defined in Eq. (47) to determine the resultant critical energy release rate G_C. For a first-order approximation, the damage mechanism matrix cracking is neglected. The deflection w_0 is estimated on the basis of a damage zone of radius $3h$. The outcomes of the local minimizations for $1, 2, \ldots, 6$ delaminations are displayed per row in Table 3 so that the global minimum can be determined in an orderly manner. For the current stacking sequence, it turns out that the increase rate of the fracture energy surpasses the increase rate of the potential energy release from two delaminations. That the minimum Λ value is found at two delaminations for both the T300/PEI and APC-2 laminates pertains to the fact that the two materials have only slight differences in elastic properties (the fiber-dominated elastic behavior). This implies that the further delamination growth calculations can be based on these two delaminations along the $-45/90$ and $90/-45$ interfaces. The formation of more delaminations is energetically unfavorable. Using the G_C values obtained, 2.6 kJ/m^2 for T300/PEI and 3.0 kJ/m^2 for APC-2, all other relevant parameters can easily be calculated by means of the closed-form equations.

Using an average membrane stiffness constant β equal to $2\pi[(1/3) + (1/\sqrt{17})]$, the load deflection curves are predicted. As shown in Fig. 7, the experimental delamination propagation curves of T300/PEI are quite smooth and exhibit a slightly nonlinear behavior. At low energy levels, the load deflection curves are accurately predicted by the linear theoretical model. At higher energy levels, the loss of accuracy resulting from the simplifications, especially the linearization and boundary condition modification, becomes larger. However, the differences remain limited and the first-order approximation appears to still be reasonably satisfactory. The APC-2 curves contain more fluctuations due to the occurrence of higher vibrational modes. It can still be observed that the theoretical propagation line follows the same trend as the experimental curves; the predicted slope, especially, is in good agreement with the measurements.

From the agreement found between the analytical and experimental load deflection curves, it is evident that the analytical model should be capable of providing an accurate prediction of the damage area, because the application of the law of conservation of energy will not introduce unacceptable inaccuracies. In Fig. 8, the damage area is plotted against the peak impact load and the impact energy. The experimental results are presented in the form of data points, and the theoretical curves are overlaid on the graphs for comparison. In the graphs of the damage area vs the peak impact load, it can be seen that the theoretical predictions for both the T300/PEI and APC-2 laminates agree well with the empirical data, despite the fact that the APC-2 measurement data show more scatter. In the graphs of the damage area vs the impact energy, there is also an excellent agreement between the analytical and experimental results for both T300/PEI and APC-2.

D. Residual Compression Strength

The residual strength calculations use the determination of the material compressive strength σ_m under the biaxial loading condition as a starting point. In the present study, the material compressive strength is extracted from the experimental ultimate strength of the

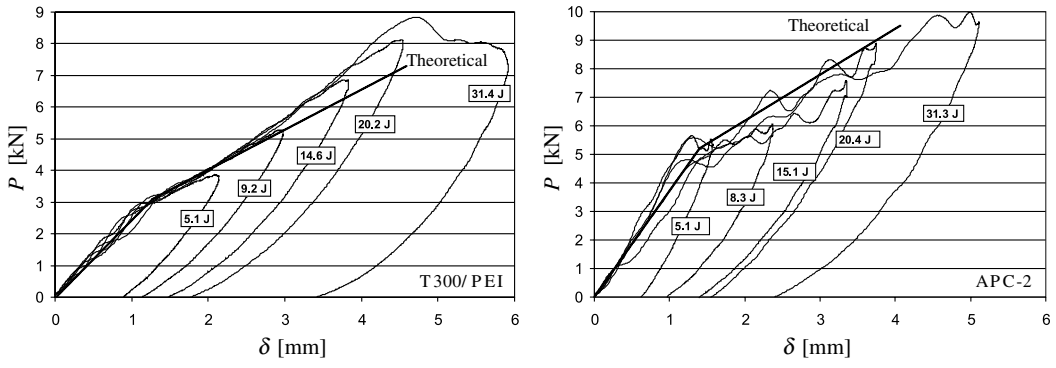

Fig. 7 Theoretical vs experimental load deflection curves.

Table 3 Calculation resultant critical energy release rate, in kilojoules per meter squared

	T300/PEI			APC-2		
n	Sublaminates	$\Lambda_{\min}$	G_C	Sublaminates	$\Lambda_{\min}$	G_C
1	$[45, 0, -45], [90_2, -45, 0, 45]$	0.1268	1.6	$[45, 0, -45], [90_2, -45, 0, 45]$	0.1466	1.8
2	$[45, 0, -45], [90_2], [-45, 0, 45]$	0.0917	2.6	$[45, 0, -45], [90_2], [-45, 0, 45]$	0.1150	3.0
3	$[45, 0, -45], [90_2], [-45], [0, 45]$	0.1079	3.5	$[45, 0], [-45], [90_2], [-45, 0, 45]$	0.1383	4.1
4	$[45, 0], [-45], [90_2], [-45], [0, 45]$	0.1231	4.4	$[45, 0], [-45], [90_2], [-45], [0, 45]$	0.1643	5.2
5	$[45], [0], [-45], [90_2], [-45], [0, 45]$	0.1497	5.5	$[45], [0, -45], [90_2], [-45], [0], [45]$	0.2023	6.4
6	$[45], [0], [-45], [90_2], [-45], [0], [45]$	0.1785	6.6	$[45], [0], [-45], [90_2], [-45], [0], [45]$	0.2443	7.7

undamaged plates. For a plate with given dimensions and layup, the buckling analysis predicts that the first buckling mode has a single half-wave in the x and y directions ($m = 1$ and $n = 1$) and that the second mode has two half-waves in the x direction and one half-wave in the y direction ($m = 2$ and $n = 1$). The accompanying critical buckling stresses of the undamaged plates of modes I and II are listed in Table 4. From the magnitudes of the critical bucking stresses, it is clear that the first mode really occurs during the tests and the higher modes are nonactive. That the mode I σ_{cr} is lower than the measured ultimate strength σ_{ult} means that the plates first buckle before the final failure. This confirms that the von Kármán postbuckling strength theory is applicable and justifies that σ_{ult} can be converted to σ_m using Eq. (71).

To illustrate the overall predictive performance of the models with regard to the impact and postimpact compression processes, the predicted and measured residual strength characteristics are displayed in Fig. 9. Because a part of the impacted specimens is cut through the middle for the cross-sectional microscopic investigation, Fig. 9 contains somewhat fewer data points compared with Fig. 8. As can be seen, both the T300/PEI and APC-2 data exhibit limited scattering, and there is a very close correlation between the theoretical and experimental results. Summarizing the previous paragraphs, all relevant quantities in the models agree with the experiments simultaneously. Although many complicating factors are removed during the development of the idealized models, the experimental verification shows that the models formed are likely sufficient to capture the most essential features, enabling fast prediction of the impact resistance and damage tolerance characteristics of laminated plates with satisfactory accuracy.

Table 4 Overview strengths

Strength, MPa	T300/PEI	APC-2
σ_{ult} experimental	264	339
σ_{cr} mode I theoretical	225	269
σ_{cr} mode II theoretical	374	443
σ_m experimental	310	427

VII. Conclusions

In the present study, analytical solutions in a relatively simple and general form have been derived and subsequently validated successfully against experiments. On the basis of the results obtained, the following conclusions can be drawn:

1) The localized deformation field, which is uncoupled from the global deformation field, appears to be appropriate for the energy release rate determination as the analysis can be significantly simplified, whereas the accuracy can be practically preserved and the error margin is known.

2) For delamination initiation analyses, it is important that the material anisotropy is accounted for in the constitutive model.

3) The lower bound of the delamination threshold load is a conservative delamination onset criterion and is therefore a useful means during the design of impact-resistant composite structures. From the experimental verification, it turns out that the average of the upper and lower bounds forms a reasonable approximation of the reality.

4) For the modeling of transverse matrix cracking, the damage-mechanics-based model for the material property degradation can be consistently integrated with the fracture-mechanics-based delamination model.

5) When establishing the energy balance in fracture analyses, the formation of multiple delaminations can be conveniently taken into consideration on the basis of the most energetically favorable configuration.

6) The membrane deformation of the damage zone leads to the stable delamination propagation, which is frequently encountered during impact testing of composite materials.

7) Neglecting higher-order effects, the resulting damage area is proven to be quadratically related to the peak impact load and linearly related to the impact energy.

8) With regard to the damage tolerance in the context of postbuckling strength reduction, the application of the energy-based stability criterion, particularly the introduction of the bending energy reduction ratio, leads to an efficient, robust, and accurate formulation of the critical buckling load of a damaged plate in relation to a perfect plate.

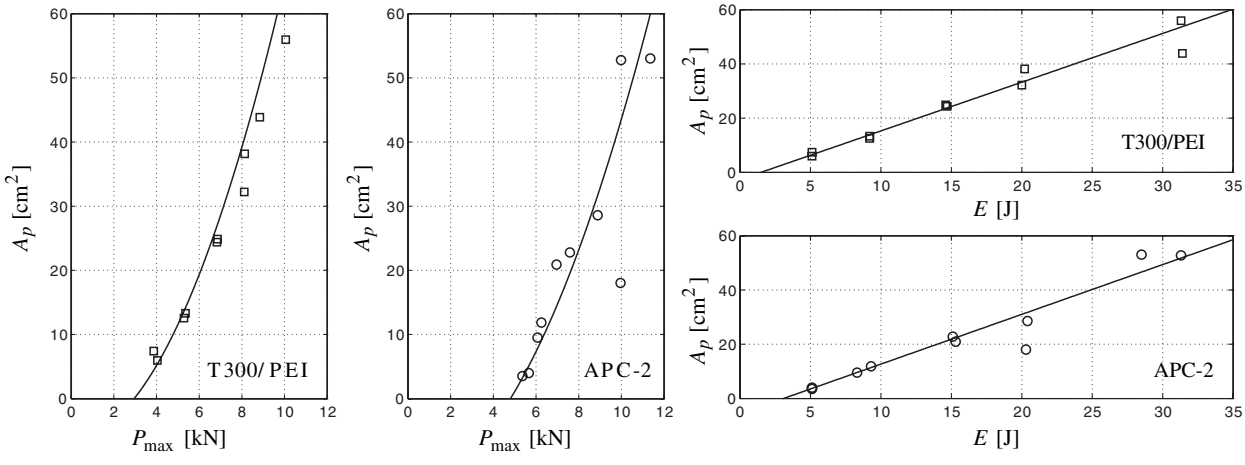

Fig. 8 Damage area as a function of the peak impact load and impact energy.

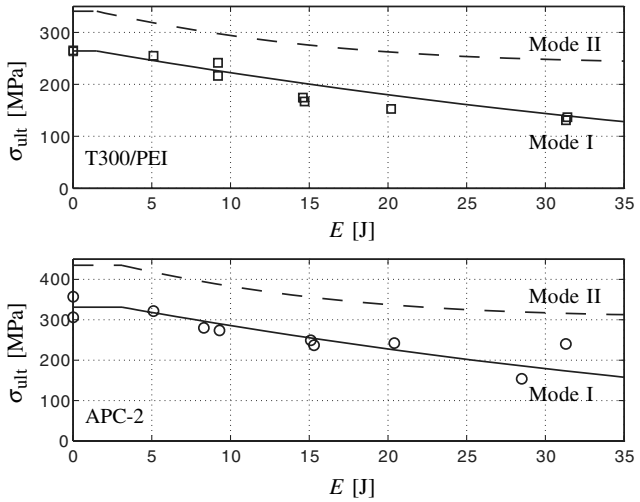

Fig. 9 Correlation between the theoretical and experimental results.

9) The analytical solutions obtained are expected to improve the fundamental understanding of the impact resistance and damage tolerance of composite structures. Because of their simplicity and accuracy, the solutions can be used as design tools to evaluate design alternatives and, in this way, accelerate the entire design process.

Appendix A: Mechanical property unidirectional prepregs

Table A1 Properties of unidirectional T300/PEI and APC-2

T300/PEI					
Elastic properties		Strength properties		Fracture properties	
E_1	119.8 GPa	X_t	1338 MPa	G_{IC}	1.2 kJ/m^2
E_2	7.8 GPa	X_c	730 MPa	G_{IIC}	1.6 kJ/m^2
G_{12}	3.5 GPa	Y_t	24 MPa	——	——
G_{23}	2.8 GPa	Y_c	151 MPa	——	——
ν_{12}	0.32	S_{12}	84 MPa	——	——
ν_{23}	0.40	——	——	——	——
APC-2					
Elastic properties		Strength properties		Fracture properties	
E_1	109.8 GPa	X_t	2050 MPa	G_{IC}	1.3 kJ/m^2
E_2	10.1 GPa	X_c	1200 MPa	G_{IIC}	1.8 kJ/m^2
G_{12}	3.7 GPa	Y_t	87 MPa	——	——
G_{23}	1.3 GPa	Y_c	230 MPa	——	——
ν_{12}	0.30	S_{12}	185 MPa	——	——
ν_{23}	0.42	——	——	——	——

Appendix B: Remaining load deflection curves

For the sake of completeness, other load deflection curves from the impact tests are shown in Fig. B1. That these results are very similar to the results already discussed demonstrates the good repeatability and reproducibility of the experiments.

Acknowledgments

The initial model was realized at the University of Twente within the framework of the BRITE/EURAM III Project, Adaptive Composite Delamination Modeling, BE-3580. A further refinement of the model was performed at Crea Mech Co., Ltd. The financial support from the European Community, the University of Twente, and Crea Mech is gratefully acknowledged. The authors would like to thank F. Eising for stimulating discussions and G.N. Heurneman for his contribution to the experimental work.

References

[1] Abrate, S., "Impact on Laminated Composite Materials," *Applied Mechanics Reviews*, Vol. 44, No. 4, 1991, pp. 155–190.

[2] Bartus, S. D., and Vaidya, U. K., "A Review: Impact Damage of Composite Materials," *Journal of Advanced Materials / Society for the Advancement of Material and Process Engineering*, Vol. 39, No. 3, 2007, pp. 3–21.

[3] Cantwell, W. J., and Morton, J., "The Impact Resistance of Composite Materials–a Review," *Composites*, Vol. 22, No. 5, 1991, pp. 347–362. doi:10.1016/0010-4361(91)90549-V

[4] Elder, D. J., Thomson, R. S., Nguyen, M. Q., and Scott, M. L., "Review of Delamination Predictive Methods for Low Speed Impact of Composite Laminates," *Composite Structures*, Vol. 66, No. 1–4, 2004, pp. 677–683. doi:10.1016/j.compstruct.2004.06.004

[5] Richardson, M. O. W., and Wisheart, M. J., "Review of Low-Velocity Impact Properties of Composite Materials," *Composites*, Vol. 27, No. 12, 1996, pp. 1123–1132. doi:10.1016/1359-835X(96)00074-7

[6] Davies, G. A. O., and Robinson, P., "Predicting Failure by Debonding/Delamination," *Debonding/Delamination of Composites*, CP-530, AGARD, Neuilly-sur-Seine, France, 1992, pp. 5.1–5.28.

[7] Olsson, R., Donadon, M. V., and Falzon, B. G., "Delamination Threshold Load for Dynamic Impact on Plates," *International Journal of Solids and Structures*, Vol. 43, No. 10, 2006, pp. 3124–3141. doi:10.1016/j.ijsolstr.2005.05.005

[8] Jones, R. M., *Mechanics of Composite Materials*, Taylor and Francis, Philadelphia, 1998.

[9] Rayleigh, L., "On the Prediction of Vibrations by Forces of Relatively Long Duration, with Application to the Theory of Collisions," *Philosophical Magazine*, Vol. 6, No. 11, 1906, pp. 283–292.

[10] Timoshenko, S., and Woinowsky-Krieger, S., *Theory of Plates and Shells*, McGraw–Hill, New York, 1959.

[11] Chang, F. K., and Lessard, L. B., "Damage Tolerance of Laminated Composites Containing an Open Hole and Subjected to Compressive Loadings: Part 1–Analysis," *Journal of Composite Materials*, Vol. 25, No. 1, 1991, pp. 2–43.

[12] Hertz, H., "Über die Berührung fester elastischer Körper," *Journal für die Reine und angewandte Mathematik*, Vol. 92, 1881, pp. 156–171.

[13] Johnson, K. L., *Contact Mechanics*, Cambridge Univ. Press, Cambridge, England, U.K., 1985.

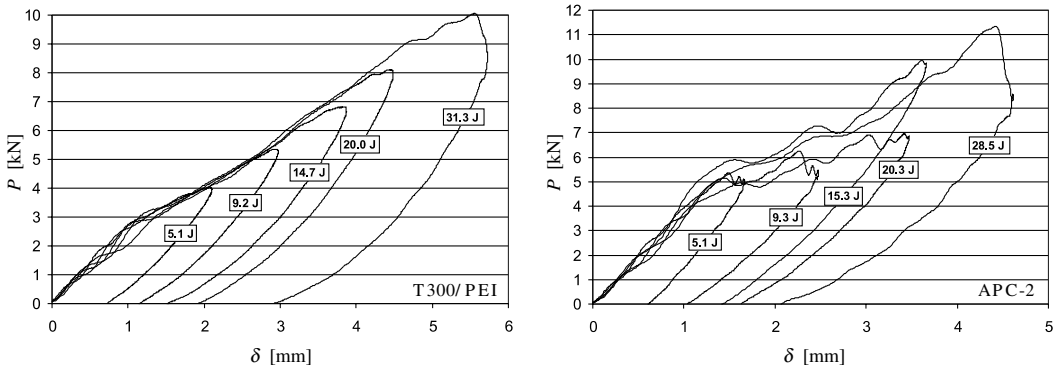

Fig. B1 Second batch of load deflection curves.

[14] Jackson, W. C., and Poe, C. C., Jr., "The Use of Impact Force as a Scale Parameter to the Impact Response of Composite Laminates," *Journal of Composites Technology and Research*, Vol. 15, No. 4, 1993, pp. 282–289.
[15] Remmers, J. J. C., and De Borst, R., "Delamination Buckling of Fibre-Metal Laminates Under Compressive and Shear Loadings," *43rd AIAA/ASME/ASCE/AHS/ASC Structures, Structural Dynamics, and Materials Conference*, AIAA, 2002.
[16] Timoshenko, S. P., and Gere, J. M., *Theory of Elastic Stability*, McGraw–Hill, New York, 1936.
[17] Brush, D. O., and Almroth, B. O., *Buckling of Bars, Plates and Shells*, McGraw–Hill, New York, 1975.
[18] Anon., "Advanced Composite Compression Tests," Boeing Specification Support Standard BSS-7260, The Boeing Company, Seattle, WA, 1988.
[19] Huang, K. Y., "On Impact Induced Delamination and Residual Compression Strength of Composite Structures," Ph.D. Thesis, Univ. of Twente, Enschede, The Netherlands, 2001.

A. Roy
Associate Editor